Supporting Information

Dynamic Self-Assembly of Ions with Variable Size and Charge in Solution

*Jana Eisermann, Andreas Kerth and Dariush Hinderberger**

Jana Eisermann, Dr. Andreas Kerth, Prof. Dr. Dariush Hinderberger
Institute of Chemistry
Martin-Luther-Universität Halle-Wittenberg
Von-Danckelmann-Platz 4, 06120 Halle (Saale), Germany
E-mail: dariush.hinderberger@chemie.uni-halle.de
web: http://www.epr.uni-halle.de/
phone: +49 (0)345 55 25230

Modifying the ionic building blocks

Phthalocyaninedihydrochloride (4^{2+})

As starting material we used 29H,31H-Phthalocyanine (Sigma-Aldrich) with a purity of 98%. In order to transform this organic compound into its correlated dihydrochloride, we dissolved the material in a 50 ml round bottom flask with dichlormethane. After sealing the round bottom flask with a rubber septum, we added hydrochloric acid ($c = 2\,\mathrm{mM}$) dissolved in diethyl ether to the stirred suspension. After six days, the precipitate was filtered, washed with diethyl ether and dried at 60°C to receive the wanted Phthalocyaninedihydrochloride.

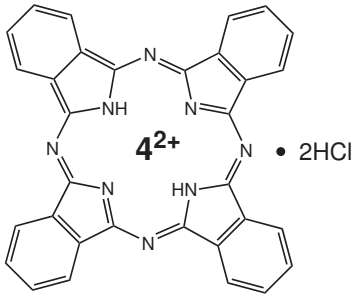

Tetrakis(4-aminophenyl)methanetetrahydrochloride (5^{4+})

We used Tetrakis(4-aminophenyl)methane (Sigma-Aldrich) with a purity of ≥95% as starting material. The same procedure as described for compound $\mathbf{4}^{2+}$ was used. After adding the hydrochloric acid ($c = 2\,\mathrm{mM}$) dissolved in diethyl ether and drying the washed filter residue, we obtained the Tetrakis(4-aminophenyl)methanetetrahydrochloride.

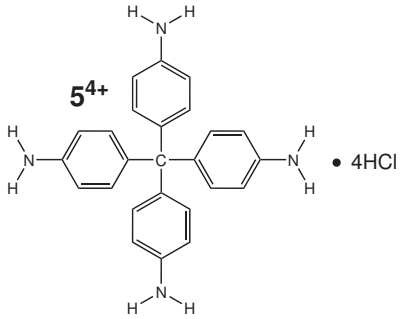

Sperminetetrahydrochloride (6^{4+})

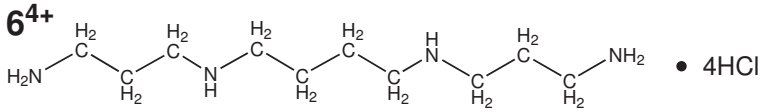

Spermine (Sigma-Aldrich) with a purity of 98% was used as starting material. Again, we added hydrochloric acid ($c = 2\,\mathrm{mM}$) dissolved in diethyl ether in order to receive the corresponding hydrochloride. After washing and drying the filter residue, we received the wanted Sperminetetrahydrochloride.

Amaranth dye (10^{3-})

The Amaranth trisodium salt (Trisodium (4E)-3-oxo-4-[(4-sulfonato-1-naphthyl)hydrazono]naphthalene-2,7-disulfonate; Sigma-Aldrich) with a purity of 85% was recrystallized. Therefore, we dissolved the starting material with a mixture of methanol:ethanol:water 6:3:1 (v/v/v) and heat the solution for one hour under constant stirring. After storing the mixture at -20°C for a couple of weeks, the precipitated Amaranth was filtered and washed with n-hexane. We received Amaranth with ≥98% purity.

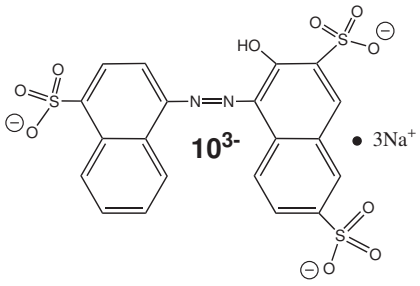

Methods

Dynamic Light Scattering (DLS) measurements

The Litesizer 500 with three different scattering angles (15°, 90°, 175°) uses a correlator, which can perform up to 248 auto/cross-correlations simultaneously over a time-range of 10 ns to 85 s. As result, we obtained the intensity time correlation function $g_2(\tau)$, which was directly fitted using a constrained regularization method incorporated inside the ALV software. The precise mathematical background of regularization DLS data is described in the CONTIN 2DP program by Provencher[1,2]. Equation S.1 shows the ALV nonlinear fit model for calculating smooth distribution functions

$$g_2(\tau) - 1 = \left(\int_{\Gamma_{min}}^{\Gamma_{max}} e^{-\Gamma\tau} \mathrm{G}(\Gamma) \mathrm{d}\Gamma \right)^2 , \tag{S.1}$$

where $\mathrm{G}(\Gamma)$ denotes the distribution function of the decay rate Γ. The decay rate itself coheres with the diffusion coefficient D through $\Gamma = Dq^2$, while $q = \frac{4\pi n}{\lambda} \sin(\frac{\theta}{2})$ describes the scattering vector including the solvent refractive index (n) and the laser wavelength (λ). Under the assumption that (i) scattering particles behave as hard spheres in dilute solution and (ii) Rayleigh-Debye theory is valid, the Stokes-Einstein-equation (equation S.2) allows calculating the distribution of the hydrodynamic radius R_H based on

$$D = \frac{k_B T}{6\pi\eta R_H} , \tag{S.2}$$

considering the Boltzmann constant k_B, the temperature T and the solvent viscosity η. The final 'mass weighted' particle radius distribution function results in adjusting the amplitudes of the decay rate in order to cut unphysically large contributions at small particle radii.

All samples were measured with a quality setup of six runs, where each run took 30 s and all runs were averaged into one intensity time correlation function. The adjustments for the laser attenuation, which have direct impact on the mean scattering intensity, were carried out automatically in order to detect optimized count rate traces.

Continuously Monitored Phase-Analysis Light Scattering (cmPALS)

The Litesizer 500 was used to perform the cmPALS experiments and to determine the zeta potential ζ during electrophoresis. However, the zeta potential cannot be measured directly and is deduced from the electrophoretic mobility μ_e of charged particles under the applied electric field.[3] The electrophoretic mobility itself is defined as

$$\mu_e = \frac{v}{E} , \tag{S.3}$$

with v as velocity of the charged particles and E as electric field strength. By techniques, which are based on electrophoretic light scattering (like PALS), the speed of the mobile particles is determined through the frequency shift between the scattered light and the original laser (Doppler shift). In short the laser beam splits into two, whereas the first part is directed towards the sample and the second part is combined or optically mixed with a modulated reference beam to determine the Doppler shift. The special feature of PALS exists in the fact that the rate of phase change between these two beams is analyzed. The newly patented method cmPALS from Anton Paar further compensates non-linearities of the modulator and the results are not affected by any longer-term deterioration in the performance of the modulator.[4]

The zeta potential ζ is calculated with the measured electrophoretic mobility μ_e by the Henry's equation (S.4)

$$\mu_e = \frac{2\varepsilon_0\varepsilon_r\zeta F(\kappa a)}{3\eta} , \tag{S.4}$$

with ε_0 as vacuum permittivity, ε_r as relative permittivity and $F(\kappa a)$ as Henry's function. The Henry's function itself depends on the thickness of the electrical double layer κ^{-1} and the particle radius a, which we replaced with the measured hydrodynamic radius R_H. To receive the actual zeta potential values, we determined the relative permittivity of our solvent mixture DMSO:glycerol:water 50:43:7 (v/v/v) as $\varepsilon_r = 54.83 \pm 1.42$ with the Keysight 16452A Liquid Text Fixture (Keysight Technologies, Santa Rosa, United States) in combination with the automatic RLC Meter RLC 300 (Grundig AG, Fürth, Germany) operating at a frequency of 10 kHz. The thickness of the electrical double layer, also known as Debye length λ_D, can be calculated with equation S.5

$$\lambda_D = \kappa^{-1} = \sqrt{\frac{\varepsilon_0\varepsilon_r k_B T}{2e^2 I N_A}} \tag{S.5}$$

applying the elementary charge e, the Avogadro's number N_A and the ionic strength I. The ionic strength inside each tested sample depence on the concentration c_i and charge z_i of the included ionic building units and can be determined with $I = \frac{1}{2}\sum c_i z_i^2$.

For the Henry's function $F(\kappa a)$ we used the approximate mathematical expression introduced by Swan and Furst[5]

$$F(\kappa a) = \frac{16 + 18\kappa a + 3(\kappa a)^2}{16 + 18\kappa a + 2(\kappa a)^2}. \tag{S.6}$$

The determined values for ionic strength and Henry's function, which were used to transfer the measured electrophoretic mobility into the final zeta potential, will be mentioned in combination with the respective system.

Continuous Wave Electron Paramagnetic Resonance (CW EPR) spectroscopy measurements

X-band CW EPR measurements, which were performed with the Miniscope MS400, made use of a sweep width of 100 G, a modulation amplitude of 600 mG and microwave attenuation of 20 dB. Note that the modulation amplitude surpassed the standard limit of $\leq 0.5\ B_{pp}$ (B_{pp} as peak-to-peak line width) to gain spectra with an improved phase resolution. Q-band CW EPR measurements were carried out with the Bruker EMX-plus spectrometer. We applied the same microwave attenuation as written before, but used a sweep width of 130 G and a modulation amplitude of 1000 mG. The important step for our simulation approach, which is based on the slow-motion theory developed by Schneider and Freed[6], was to choose suitable starting parameters for the Fremy's salt g-tensor and hyperfine coupling tensor A. The spectral simulations were performed in Matlab (R2016a, v. 9.0) exploiting the EasySpin package (v. 5.2.11)[7]. Based on literature data[8] we took the following parameter sets:

- g-tensor: $g_{xx} = 2.0086$, $g_{yy} = 2.0064$, $g_{xx} = 2.0029$
- hyperfine-tensor (X-band): $A_{xx} = 5.3\,\mathrm{G}$, $A_{yy} = 5.5\,\mathrm{G}$, $A_{zz} = 28.3\,\mathrm{G}$
- hyperfine-tensor (Q-band): $A_{xx} = 5.5\,\mathrm{G}$, $A_{yy} = 5.6\,\mathrm{G}$, $A_{zz} = 28.3\,\mathrm{G}$

Other values like line broadening and rotational diffusion rates that have to be implied into the simulation routine, depend on the discussed system and will be characterized while analyzing the CW EPR spectra. For calculating the rotational correlation time τ_c (see equation S.7), we sticked to a simple model of Brownian diffusion with an axial rotational diffusion tensor containing the values $D_{\|}$ (unique axis) and $D_{\perp}$ (perpendicular to the unique axis)[9]

$$\tau_c = \frac{1}{6\sqrt[3]{D_{\perp}^2 D_{\|}}}. \tag{S.7}$$

The discussed information about the line width of all measured CW EPR spectra (see main text) are based on isotropic broadening, which is implemented in the EasySpin program package. Note that this method does not assume any physical model causing the broadening. Instead we observed the changes of the full width at half maximum (FWHM) values of Fremy's salt with increasing concentration of

the cationic component to describe the electrostatic interactions between both ions. Furthermore, we established a routine to analyze the present anisotropy of the rotational diffusion tensor. Note that even paramagnetic molecules in the 'fast-motion regime' significantly reflect deviations from the isotropic case through their CW EPR spectra[9]. Based on the values of the rotational diffusion tensor, we calculated its anisotropy T using equation S.8

$$T = \frac{D_{\parallel} - D_{\perp}}{D_{\parallel} + 2D_{\perp}} \,. \tag{S.8}$$

A larger T-value indicates stronger separation between $D_{\parallel}$ and $D_{\perp}$, while smaller T-values reflect more isotropic tumbling, which can be attributed to weaker electrostatic interactions in the direct vicinity. For ion clouds with later self-assembly into *globular ionoids* the right balance between attractive and repulsive electrostatic forces is important, which translates into an anisotropy T that must be situated in a specific range. As reference we took the values based on the established system $\mathbf{1}^{4+}$:$\mathbf{3}^{2-}$. Finally, we had to imply so-called Euler angles α, β and γ to simulate CW EPR spectra at both frequencies with the EasySpin package. Depending on the studied cluster system, the entire set of Euler angles is made out of:

- pure $\mathbf{3}^{2-}$: $\alpha = 65°$, $\beta = 90°$, $\gamma = 15°$
- $\mathbf{1}^{4+}$:$\mathbf{3}^{2-}$: $\alpha = 85°$, $\beta = 90°$, $\gamma = 15°$
- $\mathbf{4}^{2+}$:$\mathbf{3}^{2-}$ / $\mathbf{5}^{4+}$:$\mathbf{3}^{2-}$ / $\mathbf{6}^{4+}$:$\mathbf{3}^{2-}$: $\alpha = 75°$, $\beta = 90°$, $\gamma = 15°$

UV-vis and fluorescence spectroscopy measurements

UV-vis spectra, especially for the systems $\mathbf{1}^{4+}$:$\mathbf{10}^{3-}$ and $\mathbf{6}^{4+}$:$\mathbf{10}^{3-}$, were recorded with the diode-array spectrophotometer HP 8453 (Agilent Technologies, Santa Clara, United States). Note that we had to measure a blank spectrum from the solvent mixture DMSO:glycerol:water 50:43:7 (v/v/v) before characterizing the cluster systems in order to solely display the absorption from the chromophore. Based on the explored absorption spectra of Amaranth in the systems $\mathbf{1}^{4+}$:$\mathbf{10}^{3-}$ and $\mathbf{6}^{4+}$:$\mathbf{10}^{3-}$, we could also apply fluorescence spectroscopy. Here, we utilized the Fluoromax-2 spectrometer to record the emission spectra. For each sample we took (i) three scans to improve the signal-to-noise ratio and (ii) the current lamp intensity as internal reference.
Additionally, we characterized pure $\mathbf{10}^{3-}$ ($c = 30\,\mu M$) in DMSO:glycerol:water 50:43:7 (v/v/v) to gain a reference absorption and emission spectra. Note that the dye concentration corresponds to its amount in the cluster systems. By comparing the band intensities and positions of $\mathbf{1}^{4+}$:$\mathbf{10}^{3-}$ and $\mathbf{6}^{4+}$:$\mathbf{10}^{3-}$ with our reference, we can try to link deviations here with detected globular structures from DLS data.

Ionoid evolution diagram

In this section we want to highlight the idea as well as the crafting process for the so-called ionoid evolution diagrams (IEDs), which were introduced in Ref. 10 and used in the main text. Hertzsprung-Russell diagrams that served as inspirational fundation display the classification of stars as well as stellar evolution during their complete lifetime through plotting the luminosity (often as relative value compared to our sun) on the y-axis against their surface temperature on the x-axis. Mass and time development are thus implicitely part of HRDs. Hence, these diagrams allow summarizing and displaying all stages of stellar development which is a remarkably large and complex set of data and we develop our IEDs to describe the dynamic ionic self-assembly process inside our solutions, which also comprises a wealth of complex data and long temporal evolution. To include important design elements like molar/ionic ratio, we need to define fitting parameters, which can represent the present electrostatic correlations between anionic and cationic component. Based on the fact that the source of electric fields lies in a charge or charge density[11], we plot the volume charge density of our ionoic building blocks versus their respective diameter (without a solvation shell around them).
Both parameters, diameter as well as volume charge density, were determined using the YASARA-structure software[12]. After implementing the ionic building units into the software, we applied the already existing experiment 'Energy minimization'[A] to optimize their chemical structure at a temperature of $T = 293\,\mathrm{K}$. At the end we could (i) read off the diameter and (ii) calculate the volume V (based on the molecular surface) of each ionic building unit to finally obtain the volume charge density ρ using equation S.9:

$$\rho = \frac{z^{\pm} \cdot e}{V} \quad \text{with} \quad [\rho] = \frac{\mathrm{As}}{\mathrm{m}^3}\,, \tag{S.9}$$

with $z^{\pm}$ as charge for the cationic/anionic component and e for the elementary charge. Table **S.1** summarizes for each ionic building unit the derived information from the YASARA-structure software.
After characterizing the ionic building units based on the parameters in Table **S.1**, we can illustrate the studied systems like e. g. $\mathbf{1}^{\mathbf{4}+}$:$\mathbf{2}^{\mathbf{2}-}$ in the IED by simply combining the two affected ionic compounds. Note that each possible molar/ionic ratio between both components can be highlighted as an intersection point along their connection line, as shown with the IEDs in the main text. In the next step, we want to analyze the dynamic ionic self-assembly process after the incubation time of ten days starting from the previously established intersection point. Therefore, we (i) extend the x-axis to incorporate the build up ionic structures and (ii) introduce a second y-axis that is able to describe the shape[B] of these formations. We utilize the so-called eccentricity e, which is known in mathematics as

A This experiment creates a simulation box with periodic cell boundaries around the ionic building unit. Furthermore, it applies the AMBER03 forcefield to run the simulation.

B Present deviations from a spherical structure are an important feature to distinguish between *globular ionoids* and anisotropic ionic clusters. DLS results based on different scattering angles can be used to derive these information. However, parameters like the particle form factor $P(q)$ or the ρ-ratio, which are able to describe the morphology of our ionic

Table S.1: Summary of all derived informaton from the YASARA-structure software to construct the ionoid evolution diagrams

ionic compound	diameter / nm	charge $z^{\pm} \cdot e$ / 10^{-19} As	volume V / $\mathring{A}^3$	volume charge density ρ / $10^9 \frac{\text{As}}{\text{m}^3}$
$\mathbf{1}^{\mathbf{4}+}$	1.390	6.408	907.15	0.706
$\mathbf{2}^{\mathbf{2}-}$	0.278	-3.204	118.36	-2.710
$\mathbf{3}^{\mathbf{2}-}$	0.285	-3.204	106.48	-3.010
$\mathbf{4}^{\mathbf{2}+}$	1.270	3.204	709.61	0.452
$\mathbf{5}^{\mathbf{4}+}$	0.991	6.408	528.49	1.210
$\mathbf{6}^{\mathbf{4}+}$	0.564	6.408	312.07	2.050
$\mathbf{7}^{\mathbf{2}-}$	0.245	-3.204	90.57	-3.540
$\mathbf{8}^{\mathbf{2}-}$	0.385	-3.204	144.59	-2.220
$\mathbf{9}^{\mathbf{2}-}$	0.251	-3.204	96.72	-3.310
$\mathbf{10}^{\mathbf{3}-}$	1.050	-4.806	550.85	-0.872

a measure of how much a conic section deviates from being circular, e. g. ellipses can be calculated through equation S.10

$$e = \sqrt{1 - \frac{b^2}{a^2}} \tag{S.10}$$

with $a =$ length of its semi-major axis and $b =$ length of its semi-minor axis. Circles have an eccentricity of $e = 0$, while ellipses strictly stay below the value of one. We adapt equation S.10 to characterize our three-dimensional self-assembled structures by exchanging parameter a and b with our measured hydrodynamic radii at side and back scattering. If the particle size distribution shows two separate entities, we applied the values from the smaller ones into the IED, because we want to highlight the building process of the globular structures in the sample. Note that we had to establish the following 'rule': The higher value from DLS will be set as a (semi-major axis) independent from the scattering angle. Applying equation S.10 to our DLS results, we are also able to analyze the time-dependent behavior of the self-assembled structures, e. g. the blue full dots show measurement day ten and the blue crossed dot day 43. The arrow between a pair of dots highlights the development over time and allows a better comparision between different molar/ionic ratios. At last, evolution with time is also emphasized in IEDs by the oval (or for *globular ionoids* more circular) frame.

structures more in detail, can be derived by measuring e. g. static light scattering[13].

Characteristics of solvent mixture and ionic building units

Before discussion the new systems, which we created through the substitution of the model compounds $\mathbf{1}^{4+}$ and $\mathbf{2}^{2-}$ ($\mathbf{3}^{2-}$, respectively), we want to point out the scattering behavior of the pure solvent mixture DMSO:glycerol:water 50:43:7 (v/v/v) as well as the respective ionic building units. The intensity time correlation functions at side and back scattering for the solvent itself can be found in Fig. **S.1**. After preparing the solvent mixture in the same manner like the 'real' DLS samples, we do not (i) record pronounced autocorrelation functions as well as (ii) low scattering intensities, indicating the absence of nanostructured entities inside the sample. Therefore we can conclude that the solvent mixture itself does not show tendencies for the formation of defined structures and the following intensity time correlation functions derive from introducing our ionic building units into DMSO:glycerol:water.

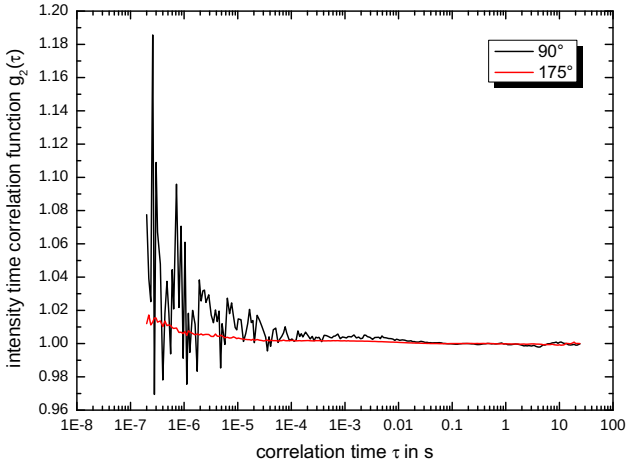

Fig. S.1: Intensity time correlation function from the pure solvent mixture DMSO:glycerol:water 50:43:7 (v/v/v) at side and back scattering.

Additionally, we measured the surface tension of our solvent mixture DMSO:glycerol:water 50:43:7 (v/v/v). Based on this value we can, considering the surface tensions of pure water and DMSO, estimate the probability of our ionic building units to move to the air-solvent interface. To determine the surface tension of our solvent mixture, we used a DCAT 21 tensiometer (DataPhysics Instruments GmbH, Filderstadt, Germany) with a Du Noüy ring setup. We inserted the ring into the solvent and applied a total of 20 cicles, where the surface tension was calculated with the respective Software SCAT 31 while pulling and pushing the created lamella into the bulk, as shown in Fig. **S.2**. Through averaging the values for the last ten cicles, we obtained a surface tension for our solvent mixture of $53.698\,\mathrm{mN/m} \pm 0.008\,\mathrm{mN/m}$. This result is much closer to pure DMSO ($43.670\,\mathrm{mN/m} \pm 0.002\,\mathrm{mN/m}$) than pure water ($72.287\,\mathrm{mN/m} \pm 0.046\,\mathrm{mN/m}$), which reduces the potential of our amphiphil building units to attach at the air-solvent interface, but to remain inside the bulk.

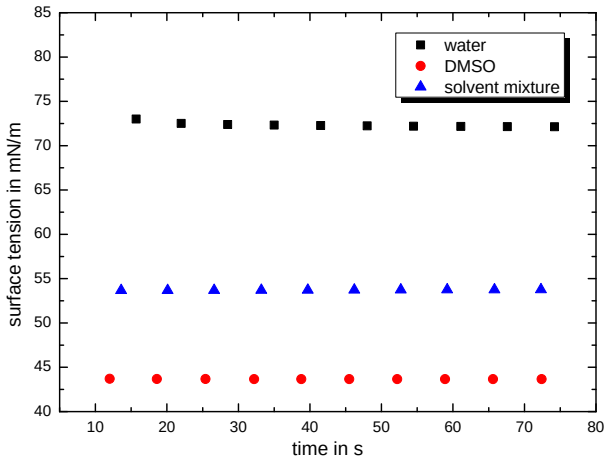

Fig. S.2: Surface tension of water, DMSO and the solvent mixture DMSO:glycerol:water 50:43:7 (v/v/v) recorded over a course of 20 cicles. The graph contains the values while pulling the Du Noüy ring setup from the air-solvent interface.

To present the DLS data for all ionic building units (which were used for DLS measurements) at side and back scattering in a combined manner, we prepared two separate panels. The first panel (see Fig. **S.3**) highlights the cationic building units $\mathbf{1}^{4+}$, $\mathbf{4}^{2+}$, $\mathbf{5}^{4+}$ and $\mathbf{6}^{4+}$ with the same concentration as used inside the tested DLS samples containing methanedisulfonate ($\mathbf{2}^{2-}$). All plots of the intensity time correlation functions are intentionally reaching 1.9 at the y-axis, because (i) it helps comparing the different building units and (ii) our model system comprises, after the initial incubation period of ten days, such well pronounced graphs. Furthermore, we wanted to highlight the y-intercept of 1.3, which marks an important indicative value for analyzing the signal-to-noise ratio of a recorded sample: If the autocorrelation functions stay below this value, then only weakly scattering particles or turbid samples are present.

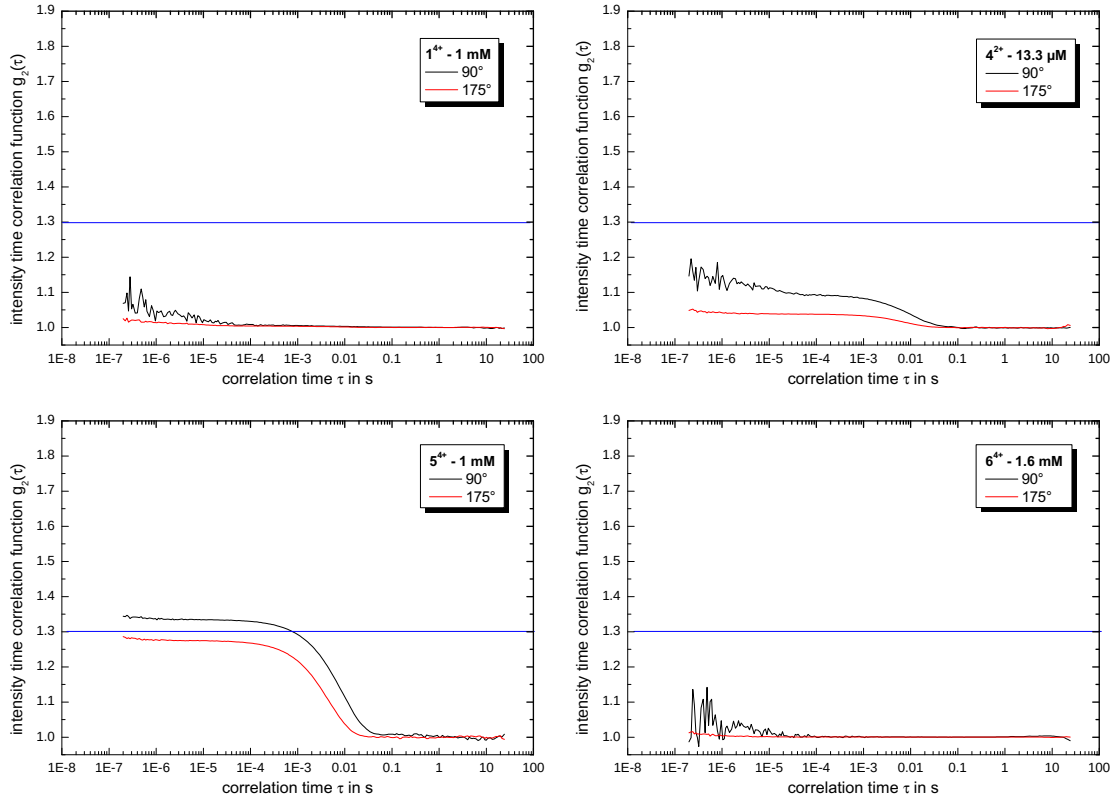

Fig. S.3: Intensity time correlation functions from the four tested cationic building units $\mathbf{1}^{4+}$, $\mathbf{4}^{2+}$, $\mathbf{5}^{4+}$ and $\mathbf{6}^{4+}$ in DMSO:glycerol:water 50:43:7 (v/v/v) at side (black line) and back (red line) scattering. The added blue lines at y-intercept value 1.3 aid as guidance and are further described in the text.

Based on the established indicative value we can conclude that only $\mathbf{5}^{4+}$-ions with a concentration of 1 mM show a high enough scattering intensity to create autocorrelation functions with a reasonable signal-to-noise ratio. Note that this cation presents in combination with methanedisulfonate less resolved scattering profiles after the incubation period of ten days, which will be discussed later on. The other cations $\mathbf{1}^{4+}$, $\mathbf{5}^{4+}$ and $\mathbf{6}^{4+}$ do not present tendencies in forming aggregates or some kind of well-defined structure inside the ternary solvent mixture and are therefore good candidates for the build up of colloid-like ionic cluster.

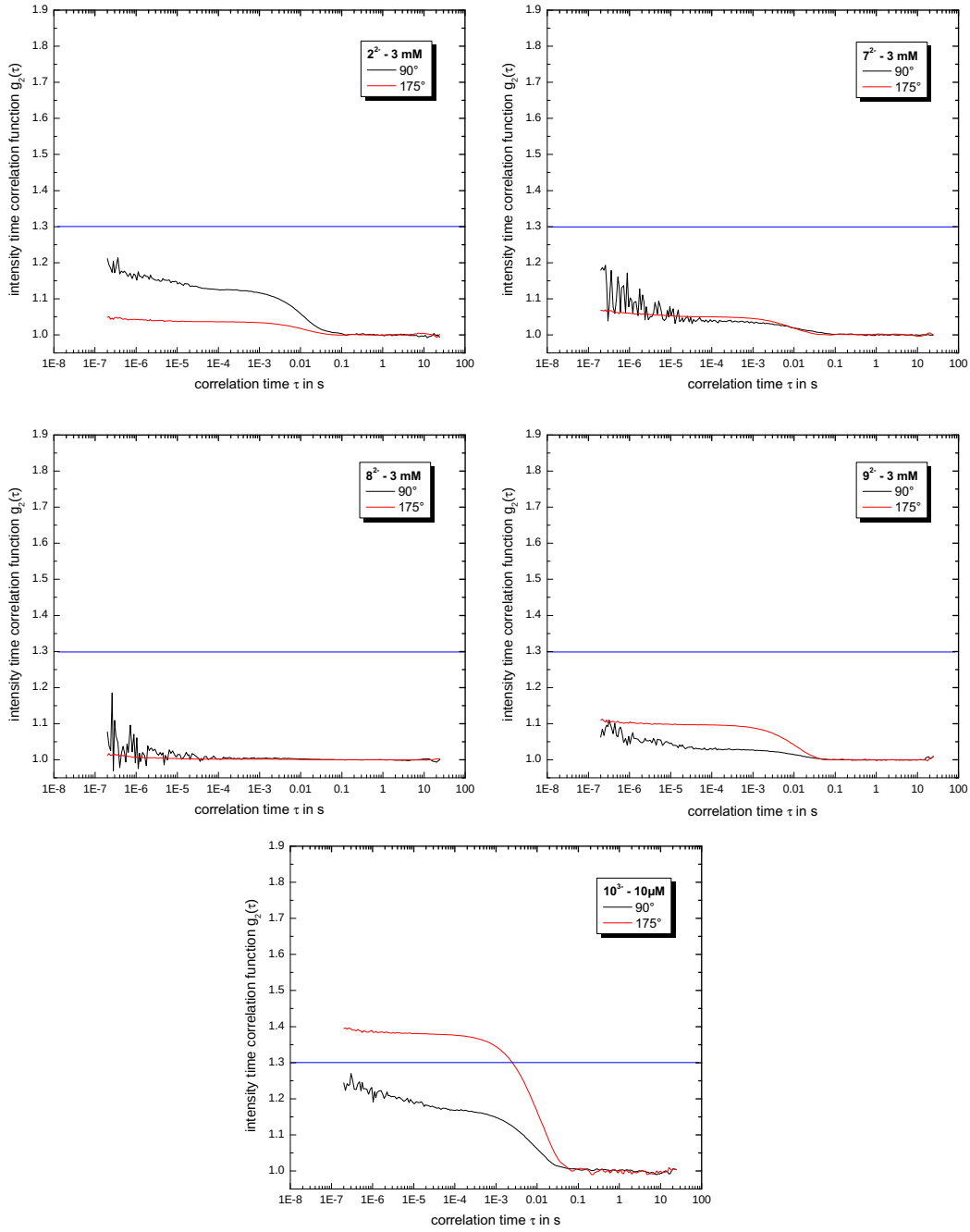

Fig. S.4: Intensity time correlation functions from the five tested anionic building units $\mathbf{2}^{2-}$, $\mathbf{7}^{2-}$, $\mathbf{8}^{2-}$, $\mathbf{9}^{2-}$ and $\mathbf{10}^{3-}$ in DMSO:glycerol:water 50:43:7 (v/v/v) at side (black line) and back (red line) scattering. The again added blue lines at y-intercept value 1.3 aid as guidance.

The second panel in Fig. **S.4** presents the anionic building units $\mathbf{2}^{2-}$, $\mathbf{7}^{2-}$, $\mathbf{8}^{2-}$, $\mathbf{9}^{2-}$ and $\mathbf{10}^{3-}$ with their respective concentration as applied in mixtures containing the 'Texas-sized molecular box'. The dianion of Fremy's salt ($\mathbf{3}^{2-}$) was not measured in this context, because we exclusively used the nitroxide radical for CW EPR spectroscopy. Based on the established 'rule' for the cationic building units we can conclude that only the relatively large trianionic chromophore $\mathbf{10}^{3-}$ shows pronounced

intensity time correlation functions. This will be considered when we describe the behavior of the systems $\mathbf{1}^{\mathbf{4}+}$:$\mathbf{10}^{\mathbf{3}-}$ as well as $\mathbf{6}^{\mathbf{4}+}$:$\mathbf{10}^{\mathbf{3}-}$. The remaining small anionic building units do not possess a high enough scattering intensity to form well resolved autocorrelation functions.

Analyze model system with cmPALS method

In this section we want i) to further characterize the zeta potential for the model system $\mathbf{1}^{\mathbf{4}+}$:$\mathbf{2}^{\mathbf{2}-}$ after the incubation period of ten days and ii) to compare these results with nanosphere size standards from Thermo Scientific. The used size standard containing polystyrene particles with a certified mean diameter of 51 nm and an approximate concentration of 1% solids. The stock solution of polystyrene particles was diluted with a mixture of deionized Milli-Q-water with sodium chloride to a final concentration of 0.02% solids and an ionic strength of $I = 10\,\text{mM}$. Fig. **S.5** shows the DLS measurement of the final probe with back scattering. The particle size distribution delivers a mean hydrodynamic radius of $R_H = 28.4\,\text{nm}$, which is in the range of the predetermined hydrodynamic diameter (50-58 nm) for these nanosphere size standards. Note that the DLS results for the model system $\mathbf{1}^{\mathbf{4}+}$:$\mathbf{2}^{\mathbf{2}-}$ are already displayed in the main text.

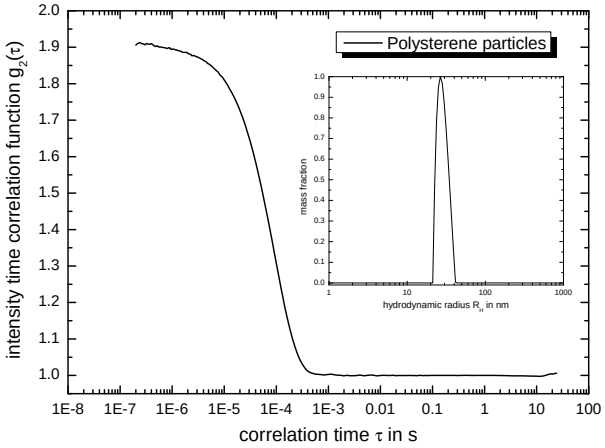

Fig. S.5: Intensity time correlation function and particle size distribution for polystyrene particles at back scattering.

After characterizing the size of the particles, we can perform cmPALS measurements to obtain the mean zeta potential for both polystyrene particles and the globular ionoids with $\mathbf{1}^{\mathbf{4}+}$:$\mathbf{2}^{\mathbf{2}-}$. Therefore, the recorded phase plots (see Fig. **S.6**) are analyzed by the Kalliope software. The slopes of the straight lines in the phase plot are directly related to the Doppler shift, which is used to determine the electrophoretic mobility of our charged entities. The visible inflection points are caused by the inversion of the electric field, leading to a change in the direction of the particle movement. The comparison of both phase plots already shows that the sign of the electrokinetic potential of the polystyrene particles and our globular ionoids must be switched. Moreover, the amplitude inside

the phase plot is more pronounced for the reference material due to their higher mobility inside the low-viscosity solvent water.

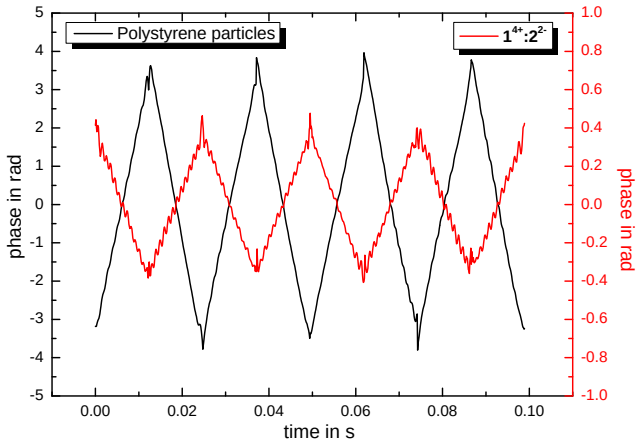

Fig. S.6: Phase plot of polystyrene particles and globular ionoids cotaining the ionic building units $\mathbf{1}^{4+}$ and $\mathbf{2}^{2-}$.

Table **S.2** combines the calculated parameters ionic strength I and Henry's function $F(\kappa a)$ with the measured electrophoretic mobility μ_e to present the actual zeta potential ζ for both samples. Note that each ionic building unit contributes, besides their main compound like $\mathbf{1}^{4+}$, counterions like PF_6^- into the final sample. Additionally, we tested the ionic building units $\mathbf{1}^{4+}$ and $\mathbf{2}^{2-}$ alone with their respective concentration of 1 mM and 3 mM to examine their mobility inside the established solvent mixture.

Table S.2: Summary of the cmPALS results with the polystyrene particles and the globular ionoids containing $\mathbf{1}^{4+}$ and $\mathbf{2}^{2-}$

compound	I / mM	$F(\kappa a)$	μ_e / $\frac{\mu mcm}{Vs}$	ζ / mV
polystyrene^{I}	10	1.101	-3.695±0.0210	-64.6±1.0
$\mathbf{1}^{4+}{}^{II}$	10	1.004	0.045±0.008	31.1±5.2
$\mathbf{2}^{2-}{}^{III}$	9	1.000	-0.001±0.003	-0.3±1.0
$\mathbf{1}^{4+}$:$\mathbf{2}^{2-}$	19	1.168	0.111±0.002	66.5±1.2

^{I}nanosphere size standards, ^{I}counterion: PF_6^-, ^{II}counterion: K^+

Substitution of 2^{2-} (3^{2-})

This section (as well as the following ones) will be divided based on the discussed systems to present additional DLS and CW EPR data as well as the UV-vis and fluorescence spectra of Amaranth-based mixtures.

$\mathbf{1}^{4+}$:$\mathbf{7}^{2-}$ ('Texas-sized molecular box':malonate)

Fig. **S.7** summarizes all intensity time correlation functions for the system $\mathbf{1}^{4+}$:$\mathbf{7}^{2-}$ with 1 mM:3 mM in the established solvent mixture. The initial phase of the self-assembly process clearly shows pronounced y-intercept-values for the autocorrelation functions, indicating potential for the formation of *ionoid*-like structures. However, their decay is also shifted to higher correlation times τ, which correlates with the build up of larger entities. Over the total measurement time we record a constant reduce for the autocorrelation function, implying the return to the initial ion cloud state. Note that we applied the ionic ratio of $^2/_3$ to directly compare $\mathbf{1}^{4+}$:$\mathbf{7}^{2-}$ to the model system $\mathbf{1}^{4+}$:$\mathbf{2}^{2-}$. The substitution of methanedisulfonate with malonate, which includes changing the sulfonate-groups with carboxylate-groups, mainly effects the stability and the shape of the self-assembled entities, as mentioned in the main text.

a) b)

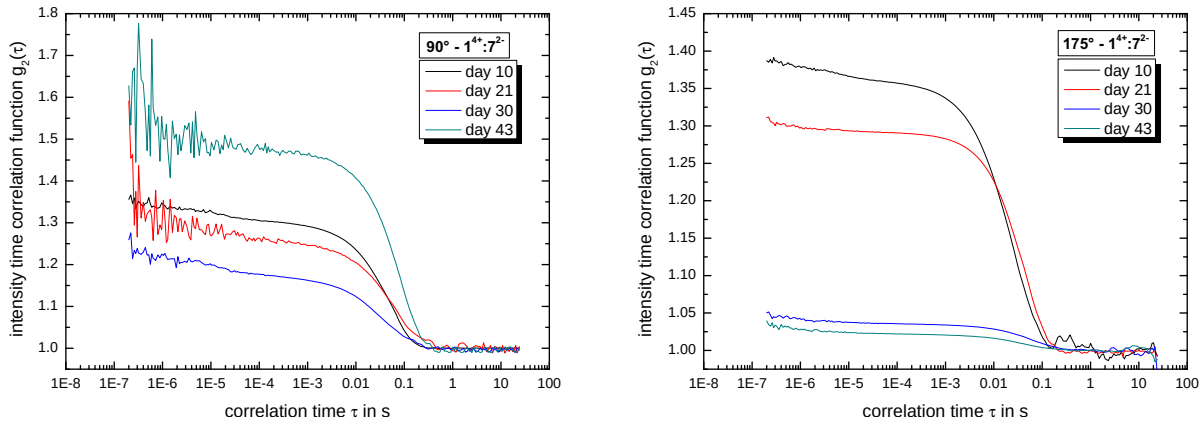

Fig. S.7: Intensity time correlation function with a) side and b) back scattering for the cluster system $\mathbf{1}^{4+}$:$\mathbf{7}^{2-}$ 1 mM:3 mM in DMSO:glycerol:water 50:43:7 (v/v/v) for all measurement days.

In Addition to the information in the main text, Table **S.3** combines the important parameter for characterizing the zeta potential for the system $\mathbf{1}^{4+}$:$\mathbf{7}^{2-}$.

Similar to the model system with methanedisulfonate, we repeated DLS measurements with this system after performing the cmPALS studies (see Fig. **S.8**). The intensity time correlation functions shows a significantly reduce for their y-intercept values, indicating a decrease in the overall scattering intensity. The partially build up anisotropic ionic cluster cannot handle the treatment with an external

Table S.3: Summary of the cmPALS results for system made out of 'Texas-sized molecular box' and malonate ($\mathbf{7}^{2-}$)

compound	I / mM	$F(\kappa a)$	μ_e / $\frac{\mu mcm}{Vs}$	ζ / mV
$\mathbf{7}^{2-}$[I]	9	1.000	-0.002±0.001	-1.7±1.0
$\mathbf{1}^{4+}$:$\mathbf{7}^{2-}$	19	1.153	0.062±0.003	37.4±2.0

[I]counterion: Na^+

electric field and therefore alter their size and shape. Due to the cmPALS treatment it seems that (in some extent) the return to the initial ion cloud state is accelerated.

a) b)

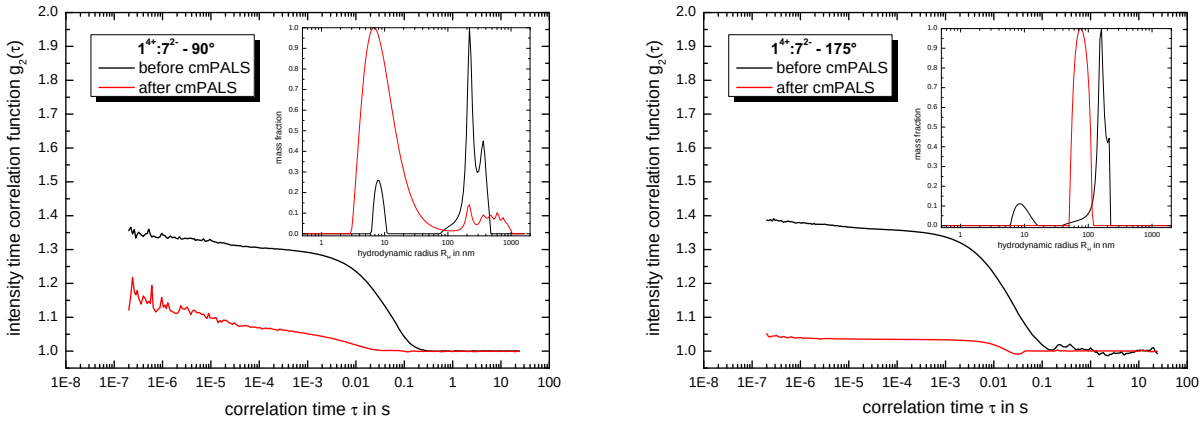

Fig. S.8: Intensity time correlation function and particle size distribution as inlay with a) side and b) back scattering for the cluster system $\mathbf{1}^{4+}$:$\mathbf{7}^{2-}$ 1 mM:3 mM in DMSO:glycerol:water 50:43:7 (v/v/v) at day 10 before and after cmPALS measurement.

$\mathbf{1}^{4+}$:$\mathbf{8}^{2-}$ ('Texas-sized molecular box':ethanedisulfonate)

Fig. **S.9** summarizes all intensity time correlation functions for the system $\mathbf{1}^{4+}$:$\mathbf{8}^{2-}$ with 1 mM:3 mM in the established solvent mixture. We detect strongly pronounced autocorrelation functions directly after the ten-day incubation period, which are already shifted to higher correlation times τ. These delayed decays stay throughout the entire measurement period, while the initial y-intercept-values of the intensity time correlation functions decrease. Compared to the model system $\mathbf{1}^{4+}$:$\mathbf{2}^{2-}$ with the same ionic ratio of $2/3$, we solely see tendencies to build up anisotropic ionic clusters. It seems that exchanging the methanedisulfonate with the slightly larger ethanedisulfonate prevents the formation of highly-defined structures with high durability due to changes in the electrostatic interactions with the 'Texas-sized molecular box'.

a) b)

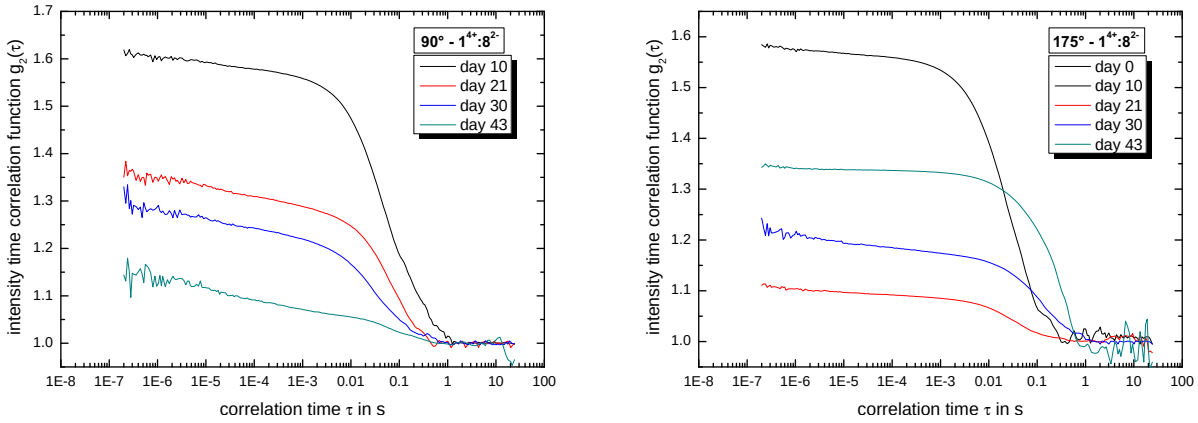

Fig. S.9: Intensity time correlation function with a) side and b) back scattering for the cluster system $\mathbf{1}^{4+}$:$\mathbf{8}^{2-}$ 1 mM:3 mM in DMSO:glycerol:water 50:43:7 (v/v/v) for all measurement days.

Table **S.4** combines the important parameter for characterizing the zeta potential for the system $\mathbf{1}^{4+}$:$\mathbf{8}^{2-}$ in a similar way compared to the system containing malonate.

Table S.4: Summary of the cmPALS results for system made out of 'Texas-sized molecular box' and ethanedisulfonate ($\mathbf{8}^{2-}$)

compound	I / mM	$F(\kappa a)$	μ_e / $\frac{\mu mcm}{Vs}$	ζ / mV
$\mathbf{8}^{2-I}$	9	1.000	-0.001±0.001	-0.7±0.7
$\mathbf{1}^{4+}$:$\mathbf{8}^{2-}$	19	1.362	0.056±0.003	28.7±1.5

^{I}counterion: Na^{+}

The direct comparison of the recorded intensity time correlation functions in Fig. **S.10** demonstrates with back scattering a significant lower y-intercept value for the measurement after the cmPALS studies. For side scattering the y-intercept stays almost constant, but the shape of the autocorrelation function changed, which leads to the detection of two distinctive peaks in the particle size distribution. Note that the pattern of the size distributions switched between both applied scattering angles, but the position of the recorded peaks remains. The system of $\mathbf{1}^{4+}$:$\mathbf{8}^{2-}$ can better cope with the influence of the electric field compared to the mixture with malonate probably due to the stronger electrostatic interactions of $\mathbf{1}^{4+}$ with the sulfonate-groups in compound $\mathbf{8}^{2-}$, as mentioned in the main text.

a) b)

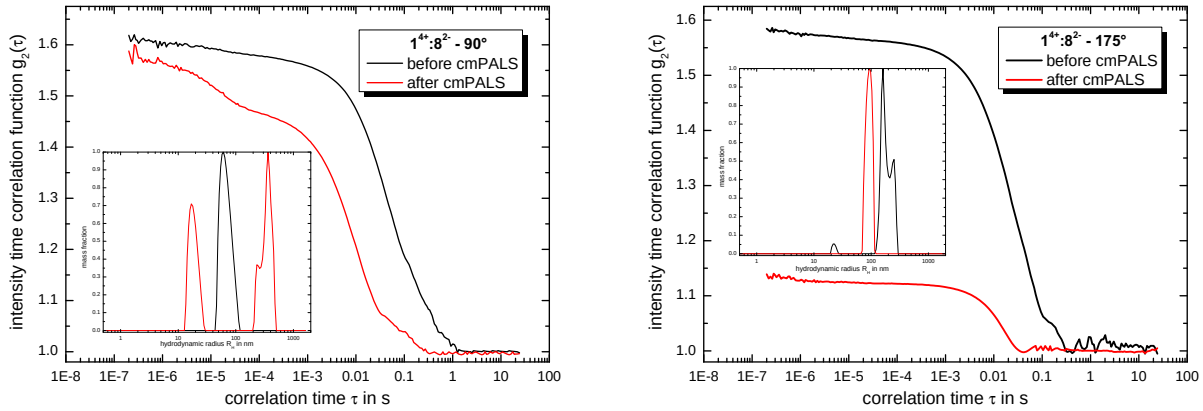

Fig. S.10: Intensity time correlation function and particle size distribution as inlay with a) side and b) back scattering for the cluster system $\mathbf{1}^{4+}$:$\mathbf{8}^{2-}$ 1 mM:3 mM in DMSO:glycerol:water 50:43:7 (v/v/v) at day 10 before and after cmPALS measurement.

$\mathbf{1}^{4+}$:$\mathbf{9}^{2-}$ ('Texas-sized molecular box':disulfate)

Fig. **S.11** summarizes all intensity time correlation functions for the system $\mathbf{1}^{4+}$:$\mathbf{9}^{2-}$ with 1 mM:3 mM in the established solvent mixture. Here, we see a similar behavior compared to the system containing $\mathbf{8}^{2-}$. Replacing methanedisulfonate with disulfate also prevents the formation of *globular ionoids*, probably due to the decomposition of the anionic component. This aspect leads to the convertion of the dianion into smaller sulfate units with just one negative charge, which can not assist the ionic self-assembly process. Note that the y-intercept value of this system is, even directly after the intial incubation period of ten days, relatively low with values around 1.3. This feature strengthen the impression of the decomposition of the disulfate over time.

a) b)

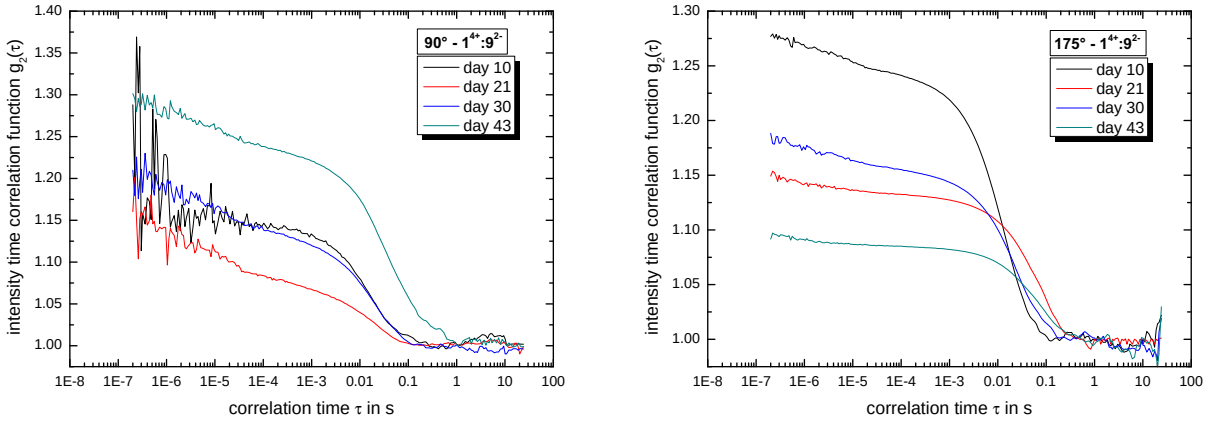

Fig. S.11: Intensity time correlation function with a) side and b) back scattering for the cluster system $\mathbf{1}^{4+}$:$\mathbf{9}^{2-}$ 1 mM:3 mM in DMSO:glycerol:water 50:43:7 (v/v/v) for all measurement days.

$\mathbf{1}^{4+}$:$\mathbf{10}^{3-}$ ('Texas-sized molecular box':Amaranth dye)

Fig. **S.12** summarizes all intensity time correlation functions for the system $\mathbf{1}^{4+}$:$\mathbf{10}^{3-}$ with concentrations 10 µM:30 µM in the established solvent mixture. The autocorrelation functions that are significantly stronger pronounced than for the pure trianionic chromophore sample (see Fig. **S.4**), present in the initial self-assembly process a shift to larger correlation times, which is more dominant for the side scattering angle. However, the y-intercept of these graphs stays rather constant, compared to the already discussed systems. We can conclude that system $\mathbf{1}^{4+}$:$\mathbf{10}^{3-}$ with a ionic ratio of $4/9$ tends to build up rather large anisotropic ionic cluster with a certain durability.

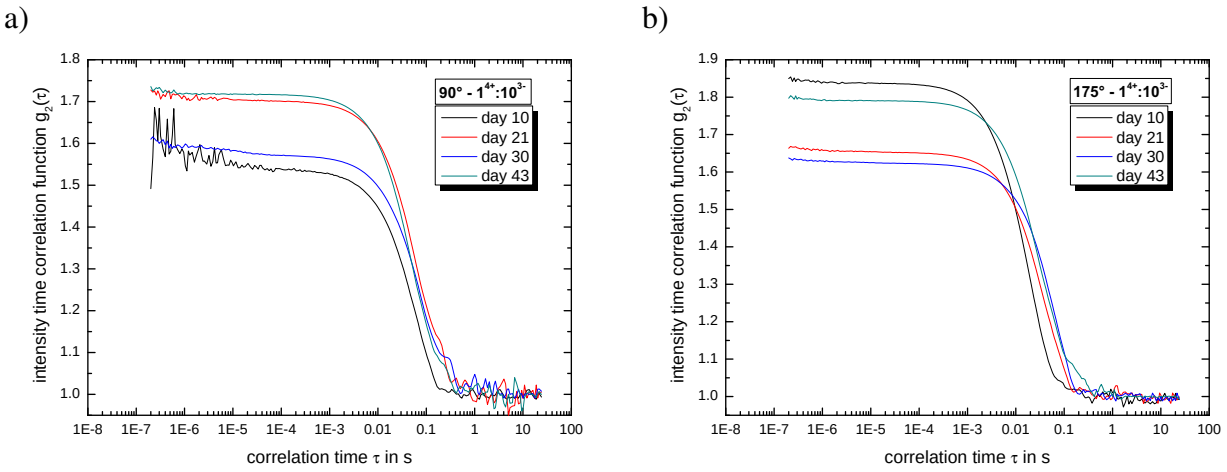

Fig. S.12: Intensity time correlation function with a) side and b) back scattering for the cluster system $\mathbf{1}^{4+}$:$\mathbf{10}^{3-}$ 10 μM:30 μM in DMSO:glycerol:water 50:43:7 (v/v/v) for all measurement days.

Based on the DLS data we can compare the recorded UV-vis and fluorescence spectra of system $\mathbf{1}^{4+}$:$\mathbf{10}^{3-}$ at each measurement day with the reference of pure Amaranth dye with $c = 30\,\mu$M, which is shown in Fig. **S.13**. Both absorption and emission band from the cluster system are, respectively, shifted by roughly 5 nm to higher wavelength indicating an influence of $\mathbf{1}^{4+}$ on the solvation shell of Amaranth. In addition, the extinction value of the absorption band slightly decreases, whereas the fluorescence intensity fluctuates throughout the total measurement time. Note that the fluorescence intensity of Amaranth significantly changes for the pure solvents DMSO, glycerol and water, making it difficult to directly correlate the detected fluctuations with the DLS data and the build up of anisotropic ionic clusters.

Substitution of $\mathbf{1}^{4+}$

$\mathbf{4}^{2+}$:$\mathbf{2}^{2-}$ (phthalcyanine:methanedisulfonate)

Fig. **S.14** summarizes all intensity time correlation functions for the system $\mathbf{4}^{2+}$:$\mathbf{2}^{2-}$ with the ratio 13.3 µM:20 µM in DMSO:glycerol:water 50:43:7 (v/v/v). One can clearly state that the decay of the

a) b)

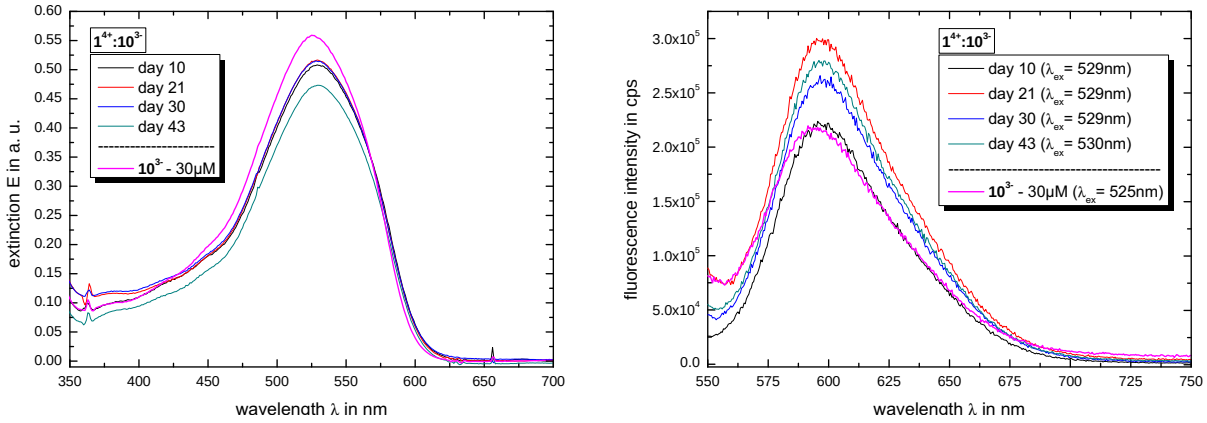

Fig. S.13: a) UV-vis spectra and b) fluorescence spectra for the cluster system $\mathbf{1}^{4+}$:$\mathbf{10}^{3-}$ 10 μM:30 μM in DMSO:glycerol:water 50:43:7 (v/v/v) for all measurement days. Both graphs show a magenta curve highlighting pure Amaranth dye with $c = 30\ \mu M$.

autocorrelation functions is slightly shifted to higher correlation times τ, but stays constant throughout all measurement days. This indicates the (partially) formation of anisotropic ionic cluster with rather robust hydrodynamic radii. However, we detect a steady decrease in the y-intercept, which indicates the starting decomposition of the self-assembled entities into more trivial ion pair coordinations.

a) b)

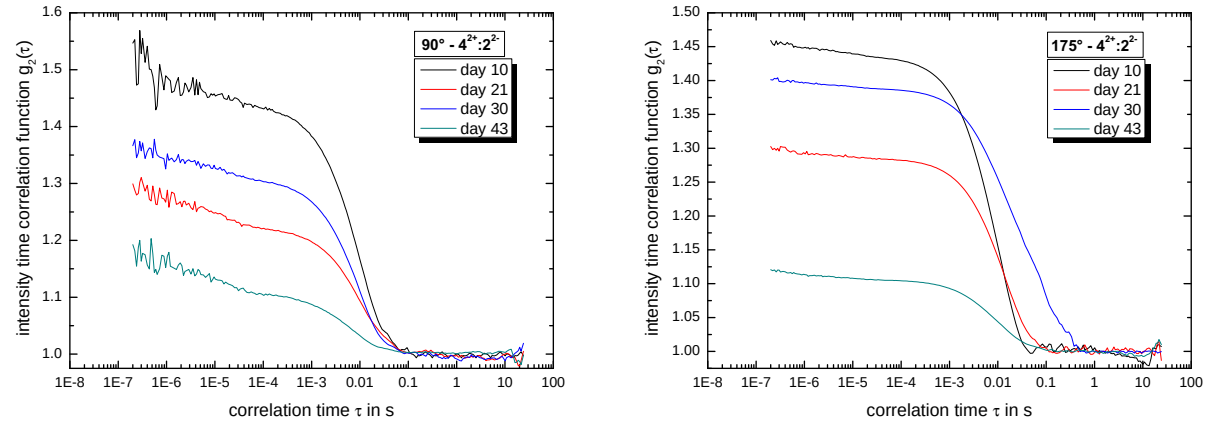

Fig. S.14: Intensity time correlation function with a) side and b) back scattering for the cluster system $\mathbf{4}^{2+}$:$\mathbf{2}^{2-}$ 13.3 μM:20 μM in DMSO:glycerol:water 50:43:7 (v/v/v) for all measurement days.

Besides DLS, we tried to apply UV-vis and fluorescence spectroscopy, but even the pure $\mathbf{4}^{2+}$ in the established solvent mixture did not present significant absorption bands, leaving CW EPR as additional method to characterize the adjusted system $\mathbf{4}^{2+}$:$\mathbf{3}^{2-}$. The measured and simulated CW EPR spectra with a fixed Fremy's salt concentration of 200 µM at both X- and Q-band frequencies are summarized in Fig. **S.15**.

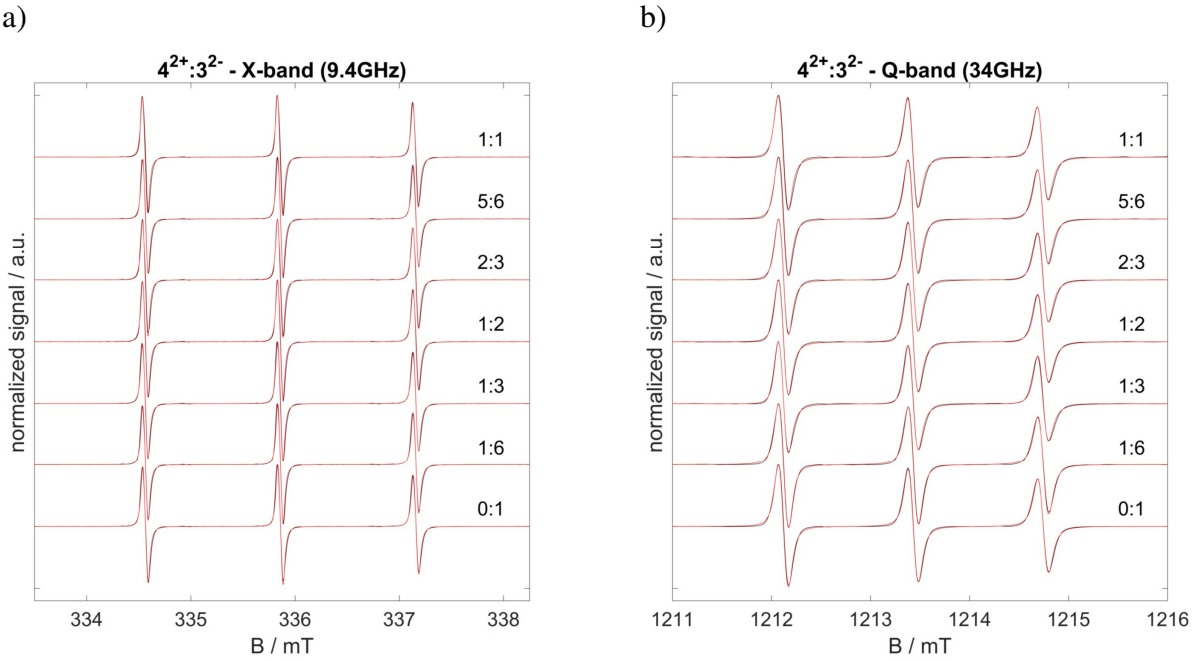

Fig. S.15: a) X-band and b) Q-band CW EPR spectra of system $\mathbf{4}^{2+}$:$\mathbf{3}^{2-}$ in DMSO:glycerol:water 50:43:7 (v/v/v) depending on the molar ratio. Both graphs show for each mixture the measured spectrum (black line) as well as the simulated spectrum (red line).

At first it seems that increasing the concentration of $\mathbf{4}^{2+}$ has no significant influence on the rotational mobility of Fremy's salt, which is also visible in the FWHM values in the main text. There are no molar ratios initiating a fixed coordination between the cationic and anionic component. Note that one reason for this behavior could be the used concentration region of 200 µM. However, we can uncover differences between the molar ratios by comparing their rotational correlation times τ_c and anisotropy T (see Fig. **S.16**). At Q-band frequencies we detect a slight increase in the rotational correlation time τ_c for molar ratios 1:3 to 5:6, indicating a slowed-down mobility of Fremy's salt due to local electrostatic interactions. In terms of anisotropy T, we just see significant changes at the globally averaged interactions and dynamics for the nitroxide based on X-band data. The reduced anisotropy beginning at molar ratio 1:2 (concentration of $\mathbf{4}^{2+}$: 100 µM) correlates with a more isotropic environment for Fremys's salt probably due to changes in its solvation shell.

a) b)

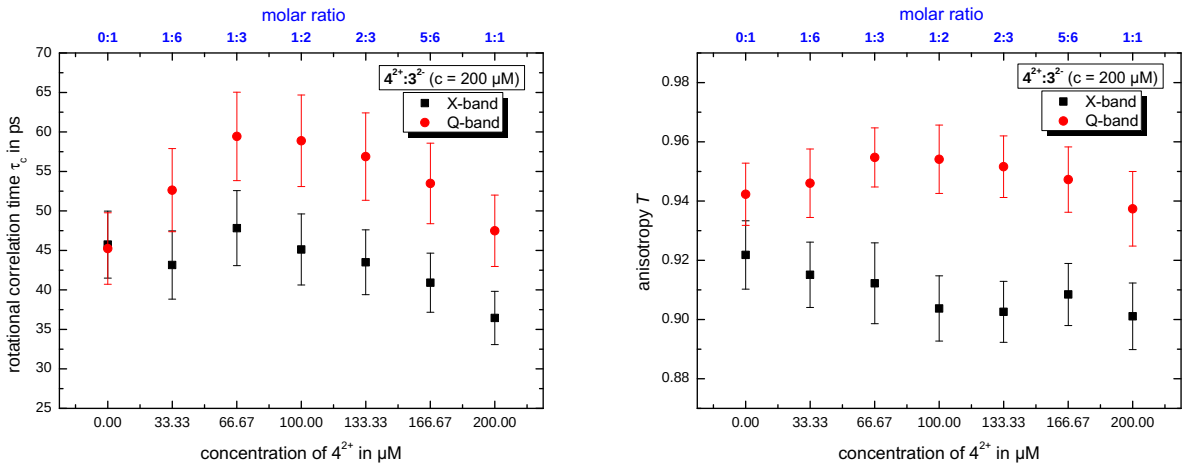

Fig. S.16: a) Rotational correlation time τ_c and b) anisotropy T of the system $\mathbf{4}^{2+}$:$\mathbf{3}^{2-}$ versus the concentration of $\mathbf{4}^{2+}$ in DMSO:glycerol:water 50:43:7 (v/v/v).

Table **S.5** summarizes the simulation results for both frequencies.

Table S.5: Summary of the simulated axial rotational diffusion tensor $D_\perp$ and $D_\parallel$ as well as the calculated rotational correlation time τ_c and anisotropy T of system $\mathbf{4}^{2+}$:$\mathbf{3}^{2-}$ in DMSO:glycerol:water 50:43:7 (v/v/v) depending on the molar ratio

ratio	X-band				Q-band			
	$D_\perp$/s^{-1}	$D_\parallel$/s^{-1}	τ_c / ps	T	$D_\perp$/s^{-1}	$D_\parallel$/s^{-1}	τ_c / ps	T
0:1	1.1e9	4.0e10	45.73	0.922	1.0e9	5.0e10	45.24	0.942
1:6	1.2e9	4.0e10	43.16	0.915	8.4e8	4.5e10	52.63	0.946
1:3	1.1e9	3.5e10	47.82	0.911	7.0e8	4.5e10	59.44	0.955
1:2	1.2e9	3.5e10	45.12	0.904	7.1e8	4.5e10	58.88	0.954
2:3	1.25e9	3.6e10	43.99	0.903	7.5e8	4.5e10	56.76	0.952
5:6	1.3e9	4.0e10	40.91	0.908	8.2e8	4.5e10	53.49	0.947
1:1	1.5e9	4.25e10	36.45	0.901	9.8e8	4.5e10	47.49	0.937

$\mathbf{5}^{4+}$:$\mathbf{2}^{2-}$ (tetrakis(4-aminophenyl)methane:methanedisulfonate)

Fig. **S.17** summarizes all intensity time correlation functions for system $\mathbf{5}^{4+}$:$\mathbf{2}^{2-}$ with 1 mM:3 mM in DMSO:glycerol:water 50:43:7 (v/v/v). We detect a fast decay of the y-intercept for the recorded autocorrelation functions at both scattering angles, indicating the fall apart of initial globular structures. Note that the y-intercept value at day ten for this system is less than for the pure $\mathbf{5}^{4+}$ solution (see Fig. **S.3**), indicating a decomposition process of the cationic component throughout the initial self-assembly for ionic cluster. Therefore, after the incubation period of ten days, the sample contains

(i) homogeneously distributed ions and (ii) ion cloud regions throughout all following measurements.

a) b)

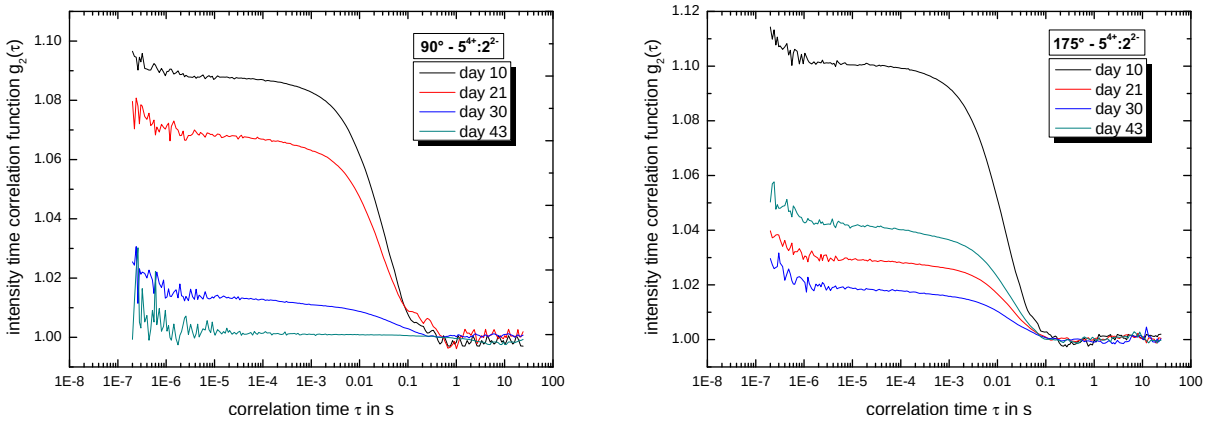

Fig. S.17: Intensity time correlation function with a) side and b) back scattering of the cluster system $\mathbf{5}^{4+}$:$\mathbf{2}^{2-}$ 1 mM:3 mM in DMSO:glycerol:water 50:43:7 (v/v/v) for all measurement days.

To further characterize the beginning of the ionic self-assembly process of compound $\mathbf{5}^{4+}$ with methanedisulfonate, we could also apply CW EPR spectroscopy with the dianion of Fremy's salt. The measured and simulated spectra with a fixed nitroxide concentration of 3 mM at both X- and Q-band frequencies are shown in Fig. **S.18**. Compared to the model system $\mathbf{1}^{4+}$:$\mathbf{3}^{2-}$, we do not see the same behavior for the rotational mobility of Fremy's salt. At X-band frequencies, the rotational correlation time τ_c slightly decreases, but the line width stays constant with increasing concentration of the cationic component. The missing increase of the FWHM values indicates the absence of strong electrostatic interactions between $\mathbf{5}^{4+}$ and $\mathbf{2}^{2-}$ for the global environment. For the local surrounding of our spin probe, which can be shown the Q-band spectra, we receive larger FWHM values due to present correlations between both components.

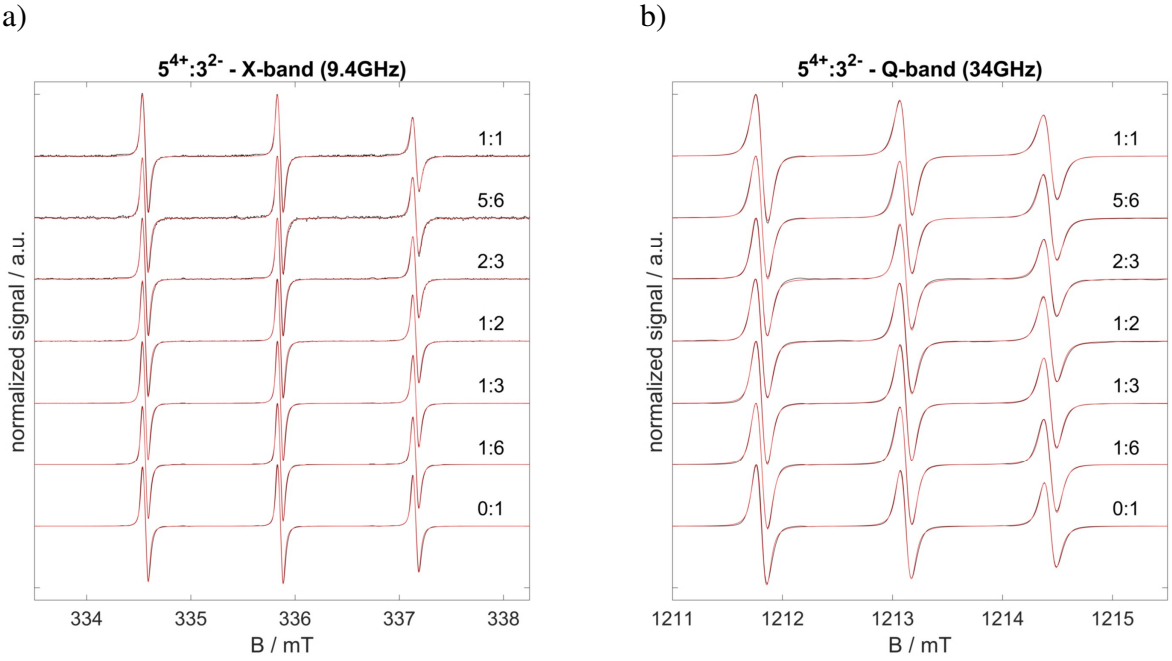

Fig. S.18: a) X-band and b) Q-band CW EPR spectra of system $\mathbf{5}^{4+}$:$\mathbf{3}^{2-}$ in DMSO:glycerol:water 50:43:7 (v/v/v) depending on the molar ratio. Both graphs show for each mixture the measured spectrum (black line) as well as the simulated spectrum (red line).

Similar to our other CW EPR measurements, we evaluate the rotational correlation time τ_c as well as the anisotropy T of the axial rotational diffusion tensor (see Fig. **S.19**). One can clearly state that the sudden decrease of T at X-band frequencies with increasing $\mathbf{5}^{4+}$ is a special feature of the cluster system. The reason for this behavior lies in the steady decrease of $D_{\|}$, whereas $D_{\perp}$ shows almost no significant changes. The adjustments of the tensor, which are vice versa compared to our model system with the 'Texas-sized molecular box', provide a possible explanation for the missing long-term stability of the colloid-like ionic structures from our DLS data.

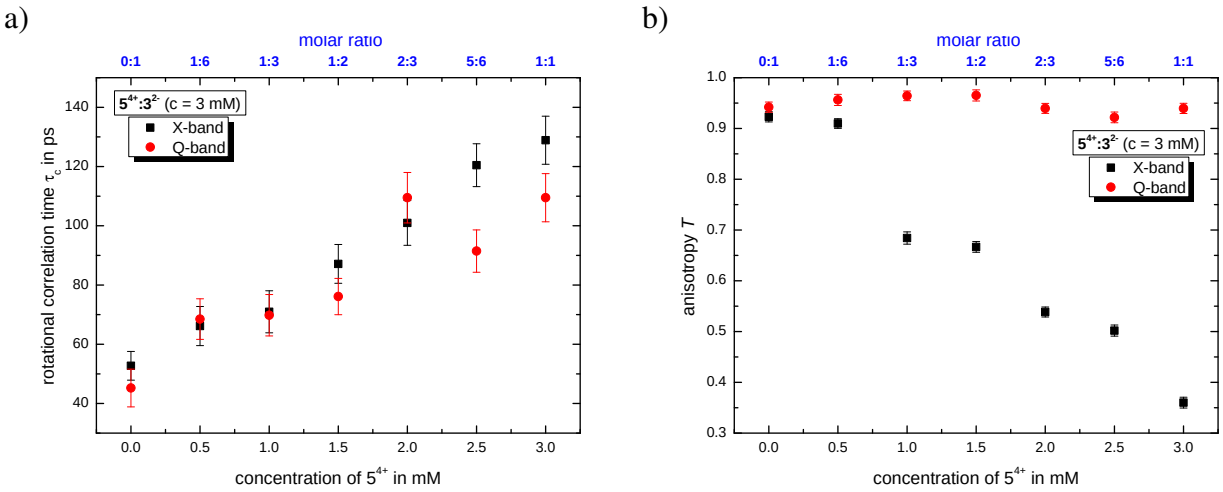

Fig. S.19: a) Rotational correlation time τ_c and b) anisotropy T of the system $\mathbf{5^{4+}}$:$\mathbf{3^{2-}}$ versus the concentration of $\mathbf{5^{4+}}$ in DMSO:glycerol:water 50:43:7 (v/v/v).

Table **S.6** combines all simulation results from X- and Q-band CW EPR spectra.

Table S.6: Summary of the simulated axial rotational diffusion tensor $D_\perp$ and $D_\parallel$ as well as the calculated rotational correlation time τ_c and anisotropy T of system $\mathbf{5^{4+}}$:$\mathbf{3^{2-}}$ in DMSO:glycerol:water 50:43:7 (v/v/v) depending on the molar ratio

ratio	X-band				Q-band			
	$D_\perp/s^{-1}$	$D_\parallel/s^{-1}$	τ_c / ps	T	$D_\perp/s^{-1}$	$D_\parallel/s^{-1}$	τ_c / ps	T
0:1	9.5e8	3.5e10	52.72	0.923	1.0e9	5.0e10	45.24	0.942
1:6	8.0e8	2.5e10	66.14	0.910	6.0e8	4.0e10	68.51	0.956
1:3	1.2e9	9.0e9	70.96	0.684	5.5e8	4.5e10	69.80	0.964
1:2	1.0e9	7.0e9	87.13	0.667	5.0e8	4.2e10	76.11	0.965
2:3	1.0e9	4.5e9	100.95	0.538	4.2e8	2.0e10	109.48	0.940
5:6	8.7e8	3.5e9	120.45	0.502	5.5e8	2.0e10	91.47	0.921
1:1	9.3e8	2.5e9	128.89	0.360	4.2e8	2.0e10	109.48	0.940

$\mathbf{6^{4+}}$:$\mathbf{2^{2-}}$ (spermine:methanedisulfonate)

Fig. **S.20** shows all intensity time correlation functions of the system $\mathbf{6^{4+}}$:$\mathbf{2^{2-}}$ with 1.6 mM:1.2 mM in DMSO:glycerol:water 50:43:7 (v/v/v). After the incubation period of ten days we recorded autocorrelation functions with high y-intercept-values for both scattering angles. Note that the decay of the recorded graphs also does not shift to larger correlation times τ, indicating the presence of colloid-like ionic structures with constant hydrodynamic radius. The partially formed anisotropic clusters (see main text) possess a certain durability, which is visible in the time-dependent

development of the y-intercept values of the intensity time correlation functions.

a) b)

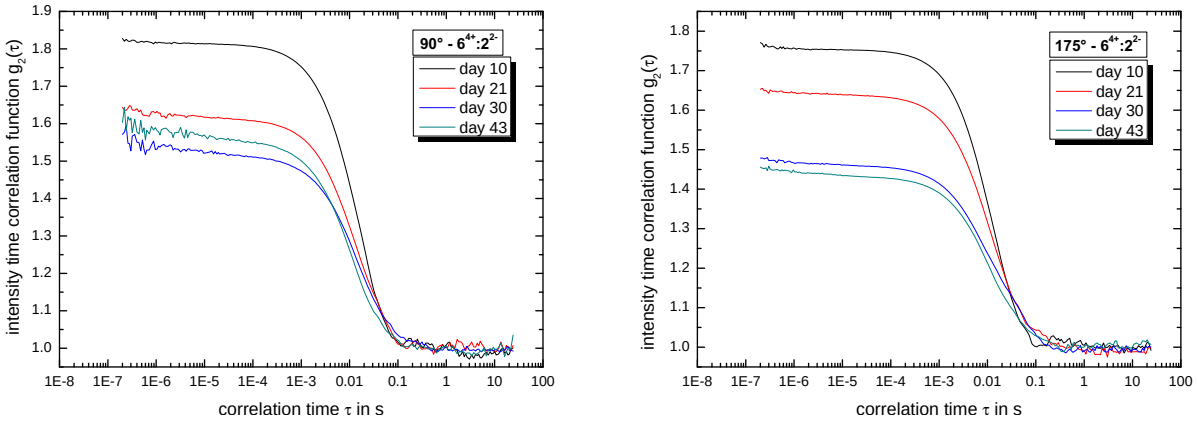

Fig. S.20: Intensity time correlation function with a) side and b) back scattering for the cluster system $\mathbf{6}^{\mathbf{4}+}$:$\mathbf{2}^{\mathbf{2}-}$ 1.6 mM:1.2 mM in DMSO:glycerol:water 50:43:7 (v/v/v) for all measurement days.

In Addition to the information in the main text, Table **S.7** combines the important parameter for characterizing the zeta potential for the system $\mathbf{6}^{\mathbf{4}+}$:$\mathbf{2}^{\mathbf{2}-}$.

Table S.7: Summary of the cmPALS results for system made out of spermine and methanedisulfonate

compound	I / mM	$F(\kappa a)$	μ_e / $\frac{\mu mcm}{Vs}$	ζ / mV
$\mathbf{6}^{\mathbf{4}+I}$	16	1.004	0.005±0.008	3.6±5.4
$\mathbf{6}^{\mathbf{4}+}$:$\mathbf{2}^{\mathbf{2}-}$	19.6	1.183	0.067±0.003	39.8±1.8

^{I}counterion: Cl^{-}

The repetitive DLS measurement with back scattering, as shown in Fig. **S.21**, displays the already mentioned decay in the y-intercept value. The overall shape of the autocorrelation function stays the same, but the particle size distribution just presents one peak, which is located between the two 'original' fractions. In combination with the result from the side scattering (see main text) we assume that the external electric field mostly affects the shape of the anisotropic ionic cluster, whereas the overall amount of self-assembled entities remains.

a) b)

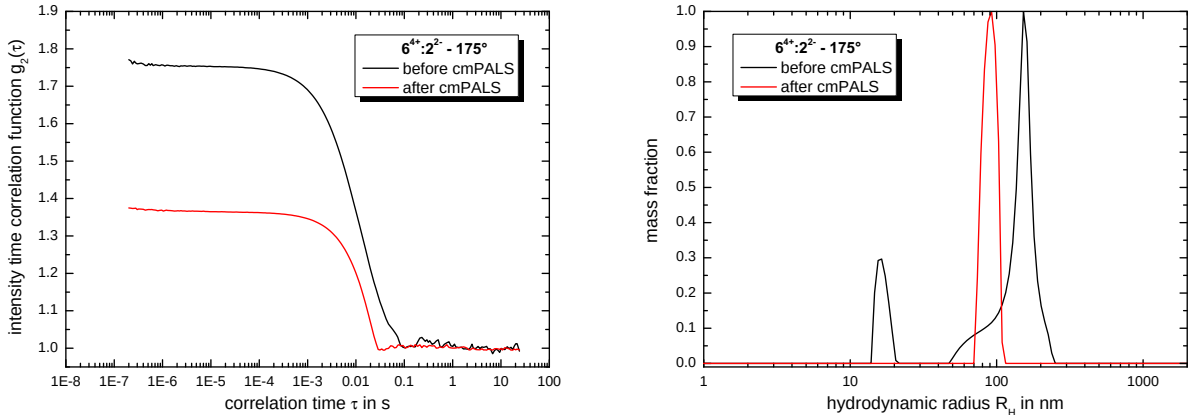

Fig. S.21: a) Intensity time correlation function and b) particle size distribution with back scattering for the cluster system $\mathbf{6}^{4+}$:$\mathbf{2}^{2-}$ 1.6 mM:1.2 mM in DMSO:glycerol:water 50:43:7 (v/v/v) at day 10 before and after cmPALS measurement.

The recorded and simulated CW EPR spectra, which are summed up in Fig. **S.22**, demonstrate a similar behavior for the rotational mobility of Fremy's salt compared to our model system $\mathbf{1}^{4+}$:$\mathbf{3}^{2-}$. X- and Q-band frequencies show a decreased rotational correlation time τ_c and increasing FWHM values with increasing concentration of the cationic component. These effects occur due to electrostatic interactions between $\mathbf{6}^{4+}$ and $\mathbf{3}^{2-}$, which are important to develop future anisotropic ionic clusters through ionic self-assembly. Note that here the electrostatic interactions with Fremy's salt are weaker compared to the 'Texas-sized molecular box'. Reasons can be the slightly lower concentration in the $\mathbf{6}^{4+}$:$\mathbf{3}^{2-}$ system or the size difference of the cationic component, leading to just anisotropic ionic clusters and not *globular ionoids*.

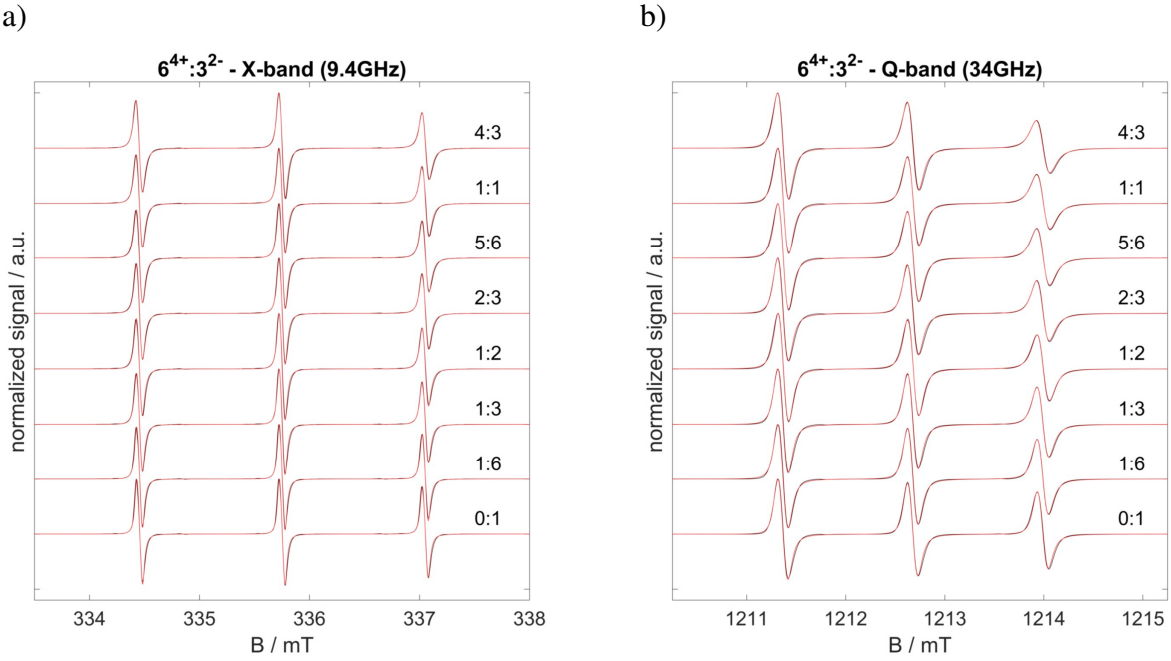

Fig. S.22: a) X-band and b) Q-band CW EPR spectra of system $\mathbf{6}^{4+}$:$\mathbf{3}^{2-}$ in DMSO:glycerol:water 50:43:7 (v/v/v) depending on the molar ratio. Both graphs show for each mixture the measured spectrum (black line) as well as the simulated spectrum (red line).

Further characterization of the axial rotational diffusion tensor are shown in Fig. **S.23**, exploiting the rotational correlation time τ_c as well as the anisotropy T. The similar behavior of the T-values at X- and Q-band frequencies indicates that the global and local environment for Fremy's salt are alike. This leads to the following conclusion: The electrostatic interactions between $\mathbf{6}^{4+}$ and $\mathbf{3}^{2-}$ in the ion cloud state dominate the direct coordination behavior of Fremy's salt. We do not reach e. g. ion pair formations with higher concentration of $\mathbf{6}^{4+}$, which happens with compound $\mathbf{1}^{4+}$. This weakend coordination in the discussed system could be the reason for partially anisotropic ionic clusters based on the DLS data.

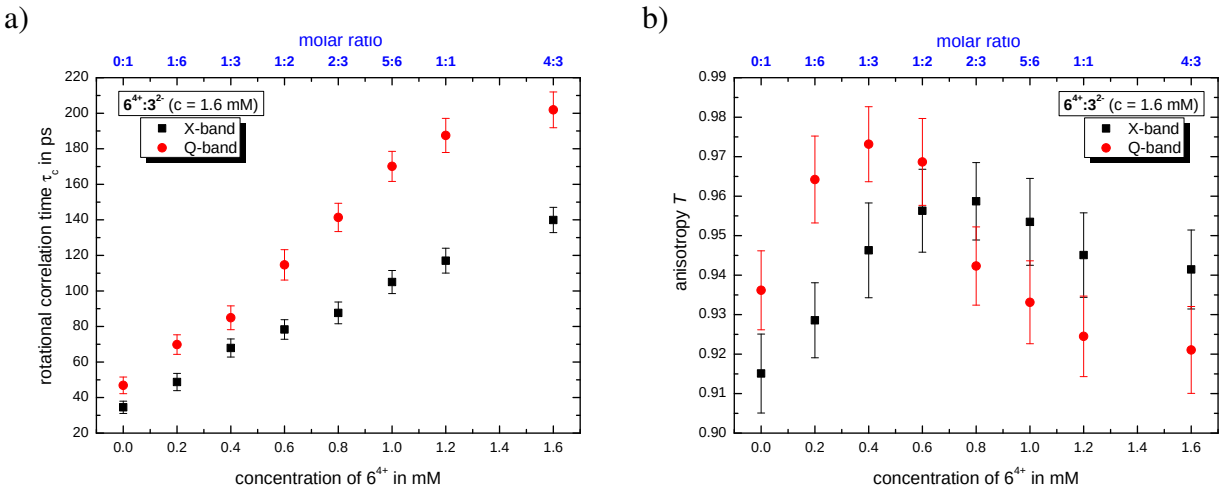

Fig. S.23: a) Rotational correlation time τ_c and b) anisotropy T of the system $\mathbf{6}^{4+}$:$\mathbf{3}^{2-}$ versus the concentration of $\mathbf{6}^{4+}$ in DMSO:glycerol:water 50:43:7 (v/v/v).

Table **S.8** completes the CW EPR data by combining the simulation results from X- and Q-band spectra.

Table S.8: Summary of the simulated axial rotational diffusion tensor $D_\perp$ and $D_\parallel$ as well as the calculated rotational correlation time τ_c and anisotropy T of system $\mathbf{6}^{4+}$:$\mathbf{3}^{2-}$ in DMSO:glycerol:water 50:43:7 (v/v/v) depending on the molar ratio

ratio	X-band				Q-band			
	$D_\perp$/s^{-1}	$D_\parallel$/s^{-1}	τ_c / ps	T	$D_\perp$/s^{-1}	$D_\parallel$/s^{-1}	τ_c / ps	T
0:1	1.5e9	5.0e10	34.52	0.915	1.0e9	4.5e10	46.86	0.936
1:6	1.0e9	4.0e10	48.74	0.929	5.5e8	4.5e10	69.80	0.964
1:3	6.5e8	3.5e10	67.90	0.946	4.1e8	4.5e10	84.90	0.973
1:2	5.25e8	3.5e10	78.29	0.956	3.2e8	3.0e10	114.65	0.969
2:3	4.6e8	3.25e10	87.64	0.959	3.2e8	1.6e10	141.38	0.942
5:6	4.0e8	2.5e10	104.99	0.953	2.8e8	1.2e10	170.09	0.933
1:1	3.8e8	2.0e10	117.04	0.945	2.65e8	1.0e10	187.51	0.925
4:3	3.25e8	1.6e10	139.92	0.941	2.5e8	9.0e9	201.90	0.921

$\mathbf{6}^{4+}$:$\mathbf{10}^{3-}$ (spermine:Amranth dye)

This mixture actually substitutes both model compounds ($\mathbf{1}^{4+}$ and $\mathbf{2}^{2-}$) at the same time, creating a inverse system based on the size ratio: small cations together with large anions. Fig. **S.24** shows all intensity time correlation functions of the $\mathbf{6}^{4+}$:$\mathbf{10}^{3-}$ with 10 µM:30 µM system in DMSO:glycerol:water 50:43:7 (v/v/v). One can clearly state that the autocorrelation functions show a large fluctuation in

their y-intercept values, indicating the formation of highly dynamic structures. The combination of small cation and large anion shows the potential to build up colloid-like ionic structures, but is not capable of stabilizing them over a longer time period.

a) b)

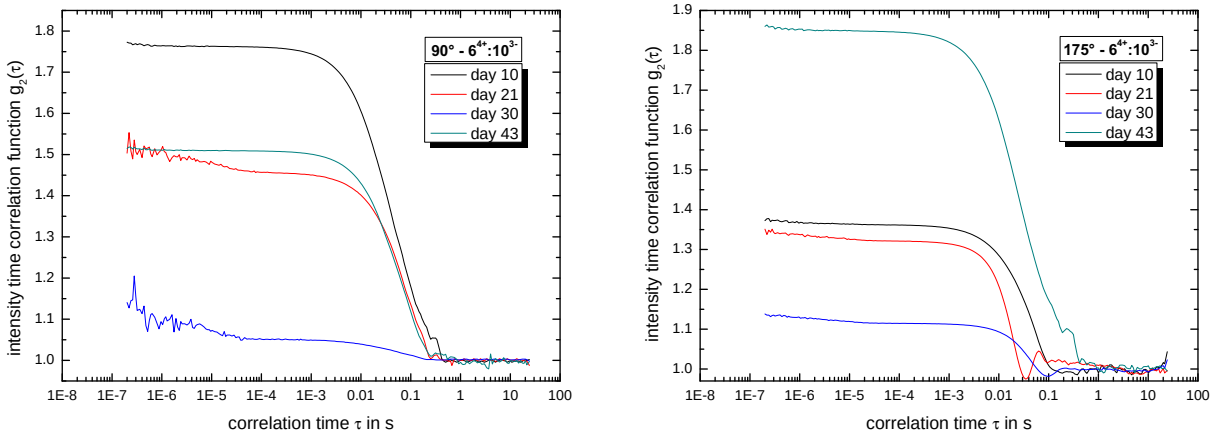

Fig. S.24: Intensity time correlation function with a) side and b) back scattering of the cluster system $\mathbf{6}^{4+}$:$\mathbf{10}^{3-}$ 10 μM:30 μM in DMSO:glycerol:water 50:43:7 (v/v/v) for all measurement days.

Possible reasons for the missing durability of anisotropic ionic cluster (or even *globular ionoids)* are (i) the low concentration ratio 10 µM:30 µM and/or (ii) too weak electrostatic interactions between both ionic compounds. We further detect through UV-vis and fluorescence spectroscopy a decrease in the absorption as well as emission band correlating to Amaranth dye (see Fig. **S.25**), indicating a steadily decomposition of $\mathbf{10}^{3-}$. This was not recorded for the system $\mathbf{1}^{4+}$:$\mathbf{10}^{3-}$, leaving the spermine as possible source for this behavior.

a) b)

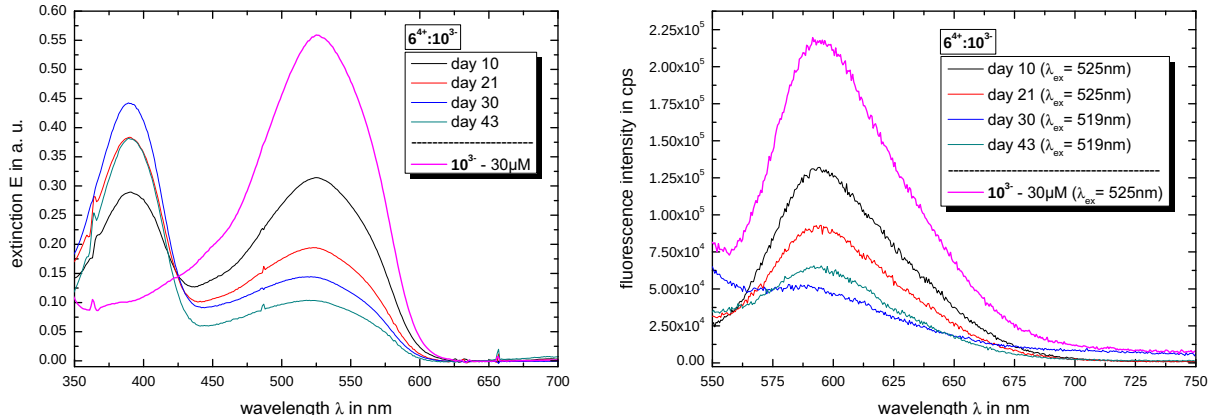

Fig. S.25: a) UV-vis spectra and b) fluroescence spectra of the cluster system $\mathbf{6}^{4+}$:$\mathbf{10}^{3-}$ 10 μM:30 μM in DMSO:glycerol:water 50:43:7 (v/v/v) for all measurement days. Both graphs show a gray curve highlighting pure Amaranth dye with $c = 30\ \mu M$.

References

1 S. W. Provencher, *Computer Physics Communications*, 1982, **27**, 213–227.

2 S. W. Provencher, *Computer Physics Communications*, 1982, **27**, 229–242.

3 S. Bhattacharjee, *Journal of Controlled Release*, 2016, **235**, 337–351.

4 C. Moitzi and B. Petrillo, *Faster, more sensitive zeta-potential measurements with cmPALS and the Litesizer 500*, Anton paar application report d51/a021 technical report, 2016.

5 J. W. Swan and E. M. Furst, *Journal of Colloid and Interface Science*, 2012, **388**, 92–94.

6 D. J. Schneider and J. H. Freed, in *Biological Magentic Resonance*, ed. L. J. Berliner and J. Reuben, Plenum Press, New York, 1989, ch. Calculating Slow Motional Magnetic Resonance Spectra, pp. 1–76.

7 S. Stoll and A. Schweiger, *Journal of Magnetic Resonance*, 2006, **178**, 42–55.

8 D. Hinderberger, *PhD thesis*, Johannes-Gutenberg-Universität Mainz, 2004.

9 D. Hinderberger and G. Jeschke, in *Site-Specific Characterization of Structure and Dynamics of Complex Materials by EPR Spin Probes*, ed. G. A. Webb, Springer, 2006, ch. Characterization of Structure and Dynamics of Complex Materials, pp. 1529–1537.

10 J. Eisermann and D. Hinderberger, *Phys. Chem. Chem. Phys.*, 2019, **21**, 1152–1159.

11 W. Demtröder, *Experimentalphysik 2 - Elektrizität und Optik*, Springer Spektrum, 2013.

12 E. Krieger, T. Darden, S. B. Nabuurs, A. Finkelstein and G. Vriend, *Proteins: Struc., Funct., Bioinf.*, 2004, **57**, 678–683.

13 W. Schärtl, *Light Scattering from Polymer Solution and Nanoparticle Dispersions*, Springer, 2007.

Table of content entry